

---

---

# A Novel Approach to Multipinhole SPECT for Myocardial Perfusion Imaging

Tobias Funk, PhD<sup>1</sup>; Dennis L. Kirch, MSEE<sup>2</sup>; John E. Koss, MS<sup>2</sup>; Elias Botvinick, MD<sup>1</sup>; and Bruce H. Hasegawa, PhD<sup>1</sup>

<sup>1</sup>Department of Radiology, University of California, San Francisco, San Francisco, California; and <sup>2</sup>Western Cardiology Research, Inc., Westminster, Colorado

---

Myocardial perfusion imaging with SPECT remains critically important for diagnosing, assessing, and evaluating treatment of coronary artery disease. However, conventional rotational SPECT suffers from prolonged study times because of relatively low detection efficiency. We therefore have investigated a multipinhole collimator that could improve the detection efficiency in cardiac SPECT by a factor 5, while providing image quality comparable to standard rotational SPECT techniques using parallel-hole collimation. **Methods:** We have measured the spatial resolution and efficiency of a 9-pinhole and a parallel-hole collimator mounted to a standard nuclear medicine  $\gamma$ -camera as a function of distance from the collimator with a point source array. The efficiency was derived by integrating the detected counts, and the spatial resolution was determined from the full width at half maximum of the detected point spread function. In addition, we generated and reconstructed projection data of a 9-pinhole collimator from a digital heart phantom with a basal lesion. We simulated 3 scenarios: single view from left anterior, 2 views from left anterior and left lateral; and 4 views that include the 2 previous views and left lateral and anterior views. **Results:** We found that the spatial resolution of the 9-pinhole collimator with 8-mm diameter pinholes was 30% poorer than that for the parallel-hole collimator, whereas the detection efficiency was increased by >10-fold. This predicts that a 9-pinhole collimator having the same spatial resolution as a parallel-hole collimator will have 5 times greater efficiency. Reconstructed data from 1 angular view of the 9-pinhole collimator showed the expected loss of spatial resolution in the longitudinal direction with reduced resolution of the basal lesion. In addition, the tomograms showed distortions in the apical region. In contrast, the reconstructed data from 2 and 4 views of the 9-pinhole collimator demonstrated good lesion definition and also produced images describing the shape and size of the heart more accurately. **Conclusion:** Our results indicate that myocardial multipinhole tomography with 2 or more views offers an image quality and spatial resolution comparable with current rotational SPECT techniques, but with the advantage of a 5-fold increase in efficiency.

**Key Words:** myocardial perfusion imaging; SPECT; multipinhole tomography; technetium; coronary artery disease

**J Nucl Med 2006; 47:595–602**

**A**mong all forms of illness, coronary artery disease (CAD) is the single greatest cause of morbidity and mortality in the United States, the Western World, and, increasingly, the world at large (1,2). Though great effort has been expended in the prevention of CAD, there also has been great progress in the treatment of the condition. Accurate diagnosis and assessment of prognostic risk are critical in guiding therapy and monitoring therapeutic response for an individual patient. Current diagnostic methods include SPECT, echocardiography, PET, CT, and MRI; each of these methods has its unique features and limitations. In recent years, MRI has shown potential to assess myocardial perfusion, but it is compromised in the presence of pacemakers, defibrillators, and other metallic devices (3,4). In addition, like myocardial PET, cardiovascular MRI remains expensive and is less accessible than SPECT (5).

It now has been thoroughly demonstrated that nuclear myocardial perfusion imaging (MPI), performed in association with either exercise or pharmacologic stress, yields clinically important and influential prognostic information beyond that of all other methods (6–9). The ability to risk-stratify CAD patients is at the basis of its clinical success (10). Nuclear MPI, in particular SPECT, obviously remains an important clinical tool (11). Furthermore, nuclear MPI has the potential to perform molecular imaging of angiogenesis, apoptosis, hypoxia, and other signatures that we expect to emerge for more sensitive assessments of myocardial disease over the next decade (12–15).

Although SPECT remains the single most important technique to assess myocardial perfusion, it suffers from relatively low detection efficiency because of its reliance on parallel-hole collimation, which prolongs the imaging study, and which impedes patient throughput and equipment use. We therefore have investigated a multipinhole imaging system, which potentially can increase the detection efficiency 5-fold compared with conventional parallel-hole collimation, and therefore can reduce the acquisition time significantly for a myocardial perfusion study.

Our approach is inspired by the resurgence of interest in multipinhole imaging in the past 2–3 y with the application of microSPECT and molecular imaging for noninvasive assessments of small animals with high detection efficiency

---

Received Jul. 20, 2005; revision accepted Nov. 18, 2005.  
For correspondence or reprints contact: Tobias Funk, PhD, 185 Berry St., Suite 350, San Francisco, CA 94107.  
E-mail: tfunk@radiology.ucsf.edu

and submillimeter spatial resolution. Impressive results have been presented by several groups (16,17) and it is apparent that multipinhole imaging is being used with great success in small animal imaging, surpassing the spatial resolution and detection efficiency of parallel-hole collimation.

For clinical imaging, multipinhole radionuclide imaging has its historical roots in coded aperture techniques first investigated for small organ imaging in the 1970s by pioneers such as Rogers and colleagues (18–20) and Barrett and coworkers (21–23). A practical innovation was introduced by Vogel et al. (24), who performed clinical MPI using a 7-pinhole collimator. This technique and other forms of longitudinal tomography were popular for clinical MPI in the 1980s (25–29), but interest waned with the advent of rotational tomography and reasons such as the following (30,31):

- (a) Angular undersampling. The 7-pinhole collimator provides only 7 angular samples, which is not sufficient to sample the heart completely, and can produce artifacts in the reconstructed image, including image distortions and a loss of spatial resolution in longitudinal direction of the heart.
- (b) Image quality. Because modern reconstruction algorithms were not available and the computing power was limited when the 7-pinhole technique was developed and being assessed clinically in the 1980s, a simplified reconstruction algorithm (ART) was used, which limited the overall image quality.
- (c) Clipping. The multipinhole collimator must be aligned properly to obtain complete projections of the heart from all 7 views. Improper positioning of the patient in relation to the collimator leads to “clipping” of the myocardial projection data, which can produce truncation artifacts in the reconstructed images.

These shortcomings have impeded the full potential of cardiovascular multipinhole imaging. In this study we have improved angular sampling of the heart with the multipinhole collimator by increasing the number of camera positions from 1 view (stationary single detector) to 2 views (stationary dual detector) and 4 views (2 positions of a dual-detector camera).

Multipinhole collimation also offers the possibility of improving spatial resolution to submillimeter levels as has been shown very impressively for the small animal imaging systems. This is important because we anticipate that these imaging systems will be required to capture important new clinical information from new molecular imaging probes now under development (12,32–34).

## MATERIALS AND METHODS

We have evaluated a 9-pinhole collimator, which had a design similar to that used in the 1980s for longitudinal tomography of the heart and which is described in more detail in the Experi-

mental Setup section. Our goal in this study was to compare the spatial resolution and efficiency of this collimator experimentally against that of a standard parallel-hole collimator. We also acquired projection data of an anthropomorphic heart phantom with both collimators using standard protocols—for example, a single-detector angular view with the 9-pinhole collimator to assess the quality of myocardial images. Finally, we evaluated the 9-pinhole collimator using computer simulation to evaluate image quality as a function of increased angular sampling obtained by additional detector views around the phantom to evaluate acquisition geometries beyond those tested using the experimental phantom studies.

## Computer Simulations and Reconstruction Algorithm

We simulated projection data using a ray-tracing program based on a pixel-driven projector developed in our laboratory. Measured and simulated data were reconstructed with a maximum-likelihood expectation maximization (MLEM) reconstruction algorithm, which was implemented using the pixel-driven projector and a backprojector.

A 3-dimensional matrix (voxel space) contained actual or simulated digitized phantom data as digital phantoms. The positions of the detector and the multipinhole collimator were defined relative to the origin of the voxel space. The configuration of the multipinhole collimator was recorded as a matrix that tabulates the geometries of the individual pinholes (e.g., pinhole diameter, angulation, opening angle, and attenuation characteristics) defined as parameters. Specific information describing the detector configuration, including its intrinsic spatial resolution and pixel format, also was specified along with the desired statistical accuracy of the data, the angular sampling, and distance from the multipinhole collimator to the center of the voxel space.

Projection data then were generated as projections from individual voxels through the pinholes of the multipinhole collimator. In these projection calculations, we accounted for the angular acceptance of the pinhole and the voxel-to-pinhole distance. In addition, the point spread function of the pinhole response was derived numerically. As a last step, the data were convolved to model the intrinsic spatial response of the detector.

We validated our computer simulation against experimental data—for example, using a  $5 \times 5$  planar array of 1.5-MBq point sources with 2-cm spacing. The array was imaged with a pinhole collimator for 130 s at a distance of 8.6 cm from the surface of the collimator. We compared the experimental count profiles with those in the simulations. The peak heights in the experimental data vary slightly due to variations in the activity of the different point sources, but overall the simulated point spread functions describe the centroid positions and the full widths at half maximum (FWHMs) of the experimental data to within 25%.

## Experimental Setup

A custom-made 9-pinhole collimator (Fig. 1A) was mounted on a standard  $\gamma$ -camera (e.g., Philips Argus) using a standard Philips collimator collar. The collimator was designed to provide 9 simultaneous projections of the myocardium that are packed efficiently onto the  $50 \times 38$  cm<sup>2</sup> active area of the detector surface (Fig. 1B). The pinholes were about 12 cm from the detector face and were arranged in a rectangular array on a pinhole plate with an area of  $30 \times 20$  cm<sup>2</sup>. The pinholes had a diameter of 8 mm and were oriented such that the central rays of the pinholes intersected at a focal point at a distance of 31.5 cm from the detector surface.

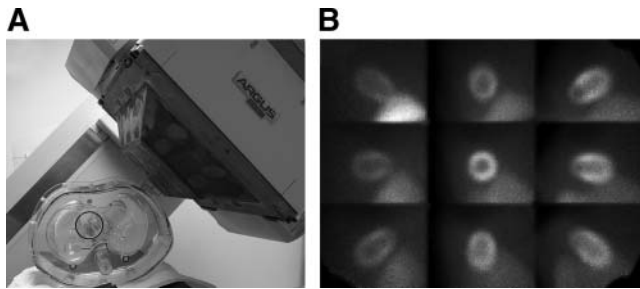


**FIGURE 1.** (A) Experimental setup for multipinhole imaging of anthropomorphic torso phantom. Camera position is at left anterior 40°. (B) Simultaneously acquired projection data of torso phantom with cardiac insert and with liver uptake with 9-pinhole collimator.

The data were acquired in list mode using a Philips (Atlas) acquisition station and were transferred to a desktop computer.

Use of the 9-pinhole collimator required calibrations for pinhole placement and for uniformity. To calibrate the system for pinhole placement, a point source was positioned at the pinhole focal point to produce 9 projections on the detector face that were backprojected to calculate the intersection points with the collimator plate. These intersection points determine experimentally derived pinhole positions as calibration parameters for the reconstruction algorithm. Furthermore, to correct for nonuniformities in the detector, a uniformity map was derived from a flood phantom placed in front of the multipinhole collimator. The uniformity map was normalized with the total number of counts and divided on a pixel-by-pixel basis to correct the projection data of the object for spatial nonuniformities.

### Comparison of Parallel-Hole Collimator and Multipinhole Collimator

We compared the performance of the 9-pinhole collimator and of a standard parallel-hole collimator in experiments intended to (a) measure relative detection efficiency and (b) evaluate the quality of images from an anthropomorphic torso phantom with cardiac insert.

**Detection Efficiency and Spatial Resolution.** As noted earlier, our goal was to demonstrate that the multipinhole method has the potential to significantly improve detection efficiency without sacrificing spatial resolution. We therefore measured the efficiency and spatial resolution characteristics of the parallel-hole collimator and the multipinhole collimator using  $^{99m}\text{Tc}$  point sources. These point sources had a diameter of 3 mm and were arranged in a  $5 \times 5$  array with 2-cm spacing. The array was placed at 10 different distances (from 4 to 20 cm) from the parallel-hole collimator and the 9-pinhole collimator, respectively, to sample the fields of view and, in particular, to sample the area where the heart would be located in an imaging study. At each position, data were acquired with the parallel-hole collimator and the 9-pinhole collimator, respectively, for 130 s. The detection efficiency was derived by integrating counts in the technetium energy window, which was set at 25%, and by summing the counts in all detector pixels. The spatial resolution was determined from the FWHM of the detected point spread function. For the multipinhole collimator the projection data of the center pinhole were used to determine the spatial resolution. The FWHM was expressed in units of millimeters in the reconstruction space.

The current 9-pinhole collimator and the parallel-hole collimator have different spatial resolutions. Therefore, we have scaled

the pinhole data to match the spatial resolution of the parallel-hole collimator.

The scaling procedure assumed that the spatial resolution of a pinhole collimator depends on the diameter of the pinhole. Thus, a smaller pinhole diameter leads to better spatial resolution. We calculated a correction factor by which the pinhole diameters must be reduced to match the spatial resolution of the parallel-hole collimator. Because the efficiency of the pinhole collimator changes as the square of the pinhole diameter, we scaled the measured efficiency of the pinhole collimator by the square of the correction factor. This procedure allowed us to compare the detection efficiencies of both collimators at the same spatial resolutions.

Our measurements were performed with a standard low-energy, general-purpose (LEGP), parallel-hole collimator. Because typical MPI studies are performed with a low-energy, high-resolution (LEHR) collimator, we also have compared the pinhole collimator with the LEHR collimator by calculating an appropriate correction factor using spatial resolution and efficiency values taken from Philips product information (35).

**Image Quality.** We evaluated image quality by performing standard imaging protocols with an anthropomorphic torso phantom using a 9-pinhole collimator and a parallel-hole collimator.

The anthropomorphic torso phantom (Data Spectrum) had a whole-body compartment with liver, lung, spine compartments, and a heart insert. The heart insert consisted of a ventricular chamber and a myocardial compartment with a separate fillable lesion having a size of about 5% of the myocardial volume and which were filled with  $^{99m}\text{Tc}$ -pertechnetate according to the values tabulated in Table 1 (36). The lesion was not filled with activity to simulate conditions associated with myocardial infarction.

First, the phantom was imaged for 15 min using a standard energy window for  $^{99m}\text{Tc}$  by positioning the 9-pinhole collimator in its normal 40° left anterior oblique position with the central view of the collimator aligned with the long axis of the left ventricle. The data were recorded, processed as described, and reconstructed using our MLEM reconstruction algorithm.

For comparison, we also imaged this phantom using a LEGP parallel-hole collimator following a standard rotational MPI protocol with 64 projections contouring the phantom across 180° (45° right anterior oblique to 45° left posterior oblique) and 25 s per stop. The projection data then were reconstructed using standard Philips autoSPECT MLEM reconstruction software (12 iterations, filtered

**TABLE 1**  
Activity Distribution in NCAT Phantom and Anthropomorphic Torso Phantom

Compartment	Activity concentration (MBq/mL)	
	NCAT phantom	Anthropomorphic phantom
Myocardium	$1.11 \times 10^{-01}$	$1.04 \times 10^{-01}$
Liver	$1.03 \times 10^{-01}$	$3.70 \times 10^{-02}$
Blood pool	$2.96 \times 10^{-03}$	$5.18 \times 10^{-03}$
Gall bladder	$8.87 \times 10^{-02}$	N/A
Lung	$5.91 \times 10^{-03}$	$5.18 \times 10^{-03}$
Kidney	$1.03 \times 10^{-01}$	N/A
Body (background)	$2.96 \times 10^{-03}$	$5.18 \times 10^{-03}$

N/A = not applicable.

backprojection first estimate), with the resulting images inspected visually for artifacts and deviations from the known geometry and activity distribution of the phantom.

### Increased Angular Sampling

As discussed earlier, the myocardium is not sampled sufficiently using only one view of a multipinhole collimator. We therefore have studied the effect of angular sampling on the image quality using our simulation program for different angular sampling strategies using the 9-pinhole collimator.

The simulation was performed with the described simulation program using the digital NCAT phantom (37,38), which models a realistic human geometry derived from MRI data of a normal patient, including the influence of background activity in liver and other organs. Cardiac and other organ geometries are parameterized, allowing changes in the phantom geometry. However, all geometric parameters have been used in standard configuration (37,38). A lateral wall lesion close to the base with 100% reduced uptake was introduced. Only one time frame of the heart cycle was generated and used for the simulations. The activity distribution was chosen according to Table 1 representing the standard activity distribution in the NCAT phantom and with the myocardial activity scaled to match that used in the anthropomorphic torso phantom.

We simulated 3 scenarios: (a) single view from left anterior 45°, (b) 2 views from left anterior 45° and left posterior 45°, and (c) 4 views that included the 2 previous views and, in addition, 2 views from 0° lateral and 90° anterior. The distance of the multipinhole collimator from the center of the heart has been chosen to contour the outline of the digital phantom. Attenuation and scatter of the  $\gamma$ -rays was omitted in this study. An acquisition time of 80 s per view was simulated and produced approximately  $6 \times 10^6$  counts per view in the simulated projection data. Appropriate Poisson noise was added to the data.

The simulated data were reconstructed with 100 iterations of the MLEM algorithm developed in our laboratory. The reconstructed images were evaluated using circumferential profile curves.

## RESULTS

### Comparison of Parallel-Hole Collimator and Multipinhole Collimator

*Detection Efficiency and Spatial Resolution.* Projection data of the  $5 \times 5$  point source phantom yielded a spatial

resolution of the LEGP collimator of 10.0 mm at 10-cm distance from the collimator. This value is in very good agreement with a system resolution of 9.4 mm at 10-cm distance as listed in the product information from Philips (35). Furthermore, the spatial resolution of the 9-pinhole collimator with 8-mm pinhole diameters is about 30% worse than that for the LEGP collimator over the range of the measured distances. Both collimators show degradation of resolution with distance from the collimator face (Fig. 2) at approximately the same rate. At a depth of 16 cm, both collimators produce a FWHM greater than the 2-cm spacing of the individual point sources.

As expected, the detection efficiency of the parallel-hole collimator changes only slightly with distance. In contrast, the measured efficiency of the 9-pinhole is relatively constant for distances from 8 to 13 cm and then decreases at distances of  $>13$  cm. For distances of  $<8$  cm, the object was not completely encompassed within the field of view of all pinholes; these points have been omitted in the graph.

The significant advantage of the pinhole collimator is apparent in Figure 2B, which shows that the efficiency for the 9-pinhole collimator is  $>10$ -fold higher but has a spatial resolution 30% poorer than that of the LEGP parallel-hole collimator. As discussed, the data can be compared more directly by scaling the efficiency of the 9-pinhole collimator for a smaller pinhole size to match the spatial resolution of the parallel-hole collimator. The scaled efficiency is about a factor 5 higher than that for the LEGP parallel-hole collimator. Typically MPI is performed with a LEHR collimator, which was not available for our experiment. However, using Philips product information, we predict that a 9-pinhole collimator with the same spatial resolution as a LEHR collimator would have a 5-fold higher detection efficiency (35).

*Image Quality.* The anthropomorphic torso phantom was imaged with a parallel-hole collimator and a multipinhole collimator to assess the image quality of both systems. The comparison of the 2 reconstructed images shows that both systems are capable of resolving the walls of the cardiac

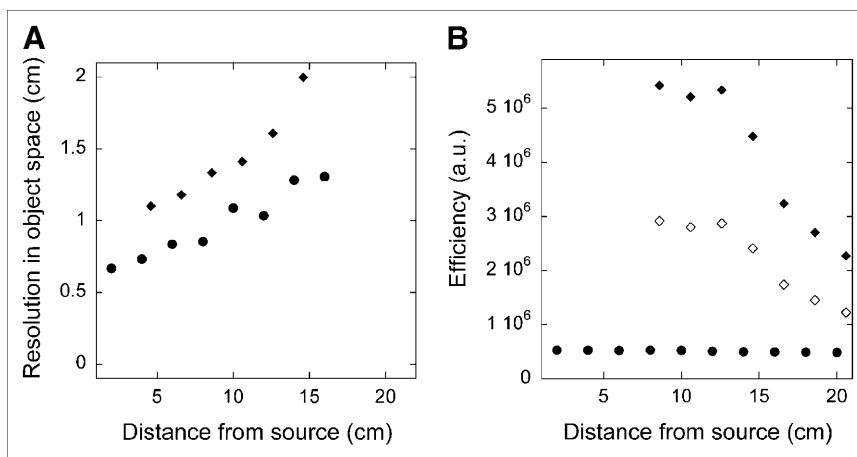


**FIGURE 2.** Spatial resolution (A) and detection efficiency (B) for LEGP parallel-hole (●) and 9-pinhole collimator (◆). ◇ depicts efficiency of 9-pinhole collimator at same spatial resolution as parallel-hole collimator. a.u. = arbitrary units.

insert within the phantom (Fig. 3). Also, the liver uptake and the cold myocardial lesion are well resolved in the short-axis views of the reconstructions.

However, in comparison with the parallel-hole collimator, the performance of a single view of the 9-pinhole collimator exhibits a substantial loss in spatial resolution in the longitudinal direction of the heart, and the myocardial lesion is not well resolved in the long-axis views. Furthermore, the myocardial image is distorted especially at the apex with the 9-pinhole collimator. Whereas the reconstructed image of the parallel-hole collimator reproduces the round shape and uniform activity of the apex, the reconstructed image of the multipinhole collimator produces a pointed image of the apex with nonuniform uptake. These artifacts are produced by the limited angular sampling obtained with the stationary, single-view multipinhole collimator, and reveal one reason why rotational tomography with parallel-hole collimators is widely used clinically. However, in our simulation studies, we show that the artifacts and distortions associated with stationary multipinhole imaging can be substantially reduced by acquiring projection data with multiple views of the multipinhole collimator.

### Simulated Projection Data of 9-Pinhole Collimator

Projection data from various angles have been simulated using the digital NCAT phantom and were reconstructed to evaluate the effect of increased angular sampling on the quality of the images obtained with multipinhole tomography.

The reconstructed images and slices of the digital phantom are presented in Figure 4. The reconstructions from the single-view, 2-view, and 4-view acquisitions resolve the liver and both the right and the left myocardial walls. However, the tomograms produced with a single view of the multipinhole collimator have poorer image quality than those produced from multiple-view acquisitions. For example, the single-view acquisition produced a reconstruction in which the apex

has a pointed, rather than a rounded, shape with a nonuniform activity distribution and with a loss of spatial resolution in longitudinal direction. For example, the left atrium is not resolved and the defect is less pronounced compared with the reconstructions with more views. These artifacts are very similar to those observed in the experimental data (Fig. 3) and underscore the validity of the simulation.

The reconstruction from 2 views shows considerable improvement in terms of the image quality compared with the reconstructions from a single view. The apex does not show the pointed shape observed with 1 view and more accurately reconstructs the shape of the digital phantom. Slight nonuniformities are visible in the apex, but the images overall are very well resolved. Reconstructions from 4 views accurately exhibit a round apex as is visible in the digital phantom and show improved spatial resolution in longitudinal direction with improved lesion definition in the long-axis view.

Figure 5 compares the circumferential profile curves from a short-axis slice containing the lesion for the reconstruction and from the corresponding slice of the digital phantom. The profile curve of the 1-view reconstruction follows that from the digital phantom reasonably well. However, the curve overshoots its known values from the phantom in 2 areas and the lesion appears as a 70% defect consistent with the previously observed loss in spatial resolution in longitudinal direction. Profile curves of the 2- and 4-view reconstructions track the profile curve of the phantom with an accuracy error of  $\pm 20\%$ . The lesion was reconstructed accurately in both cases with slightly improved accuracy obtained from the 4-view versus the 2-view reconstruction.

We find that the image quality of the tomograms improves with the number of views of the multipinhole collimator and conclude that at least 2 views of the multipinhole collimator are necessary to obtain image quality comparable with the image quality obtained from parallel-hole collimators.

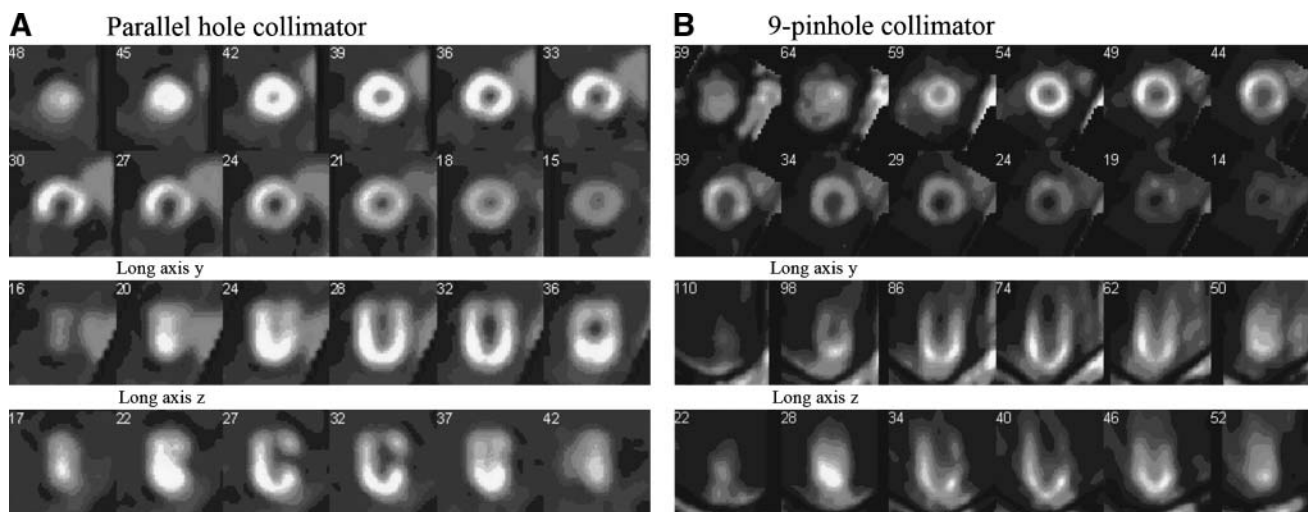
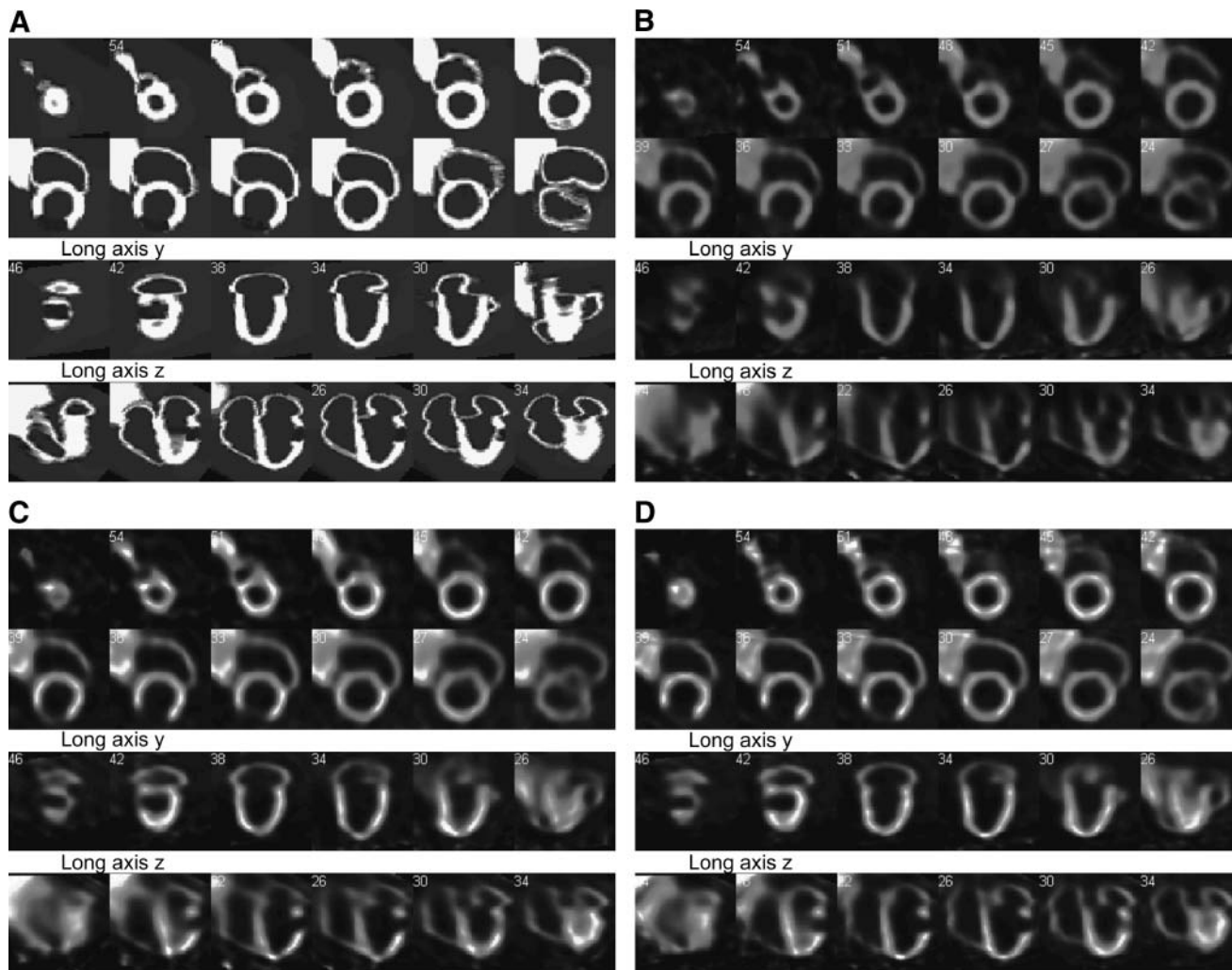


FIGURE 3. Reconstruction of projection data measured with parallel-hole collimator (A) and 9-pinhole collimator (B).



**FIGURE 4.** (A) Activity distribution in NCAT phantom. (B) Tomogram reconstructed from 1 view of 9-pinhole collimator. (C) Tomogram reconstructed from 2 views. (D) Tomogram reconstructed from 4 views.

## DISCUSSION

MPI with rotational SPECT is a well-established and important technique for diagnosis and risk stratification of patients with CAD. Millions of studies are performed each year, indicating the significant clinical need addressed by this methodology. Despite its success, MPI SPECT and SPECT in general are currently limited by detection efficiency in conjunction with prolonged study times and relatively low spatial resolution impeding even wider use of this approach.

Multipinhole imaging offers a potentially important step toward the development of enhanced imaging systems for myocardial perfusion SPECT that will combine high detection efficiency with high spatial resolution.

Our study predicts that a multipinhole imaging system can be built with spatial resolution comparable to that of parallel-hole collimators but with 5-fold higher detection efficiency. Although these results are very encouraging, further experimental studies using multipinhole collimators with matched spatial resolution are necessary.

However, the predicted higher detection efficiency should shorten the acquisition times needed to perform MPI studies from currently 15–20 min to 4–5 min, which thereby would improve patient comfort and reduce the possibility of patient motion during the examination (and thereby contribute to improved image quality and diagnostic accuracy). The improved detection efficiency could be used to shorten scan time, to improve patient throughput, and would reduce the cost of the procedure. We recognize that this is a preliminary assessment and that further studies are necessary. In particular, noise propagation in the different reconstruction algorithms, different collimator designs, and different angular sampling characteristics certainly can have different noise propagation characteristics. We therefore recognize that a more careful investigation of the statistical characteristics of the reconstructed images will be necessary to determine the ultimate role of these different approaches in MPI.

As pointed out earlier, patient positioning is extremely important for multipinhole imaging to avoid artifacts due to

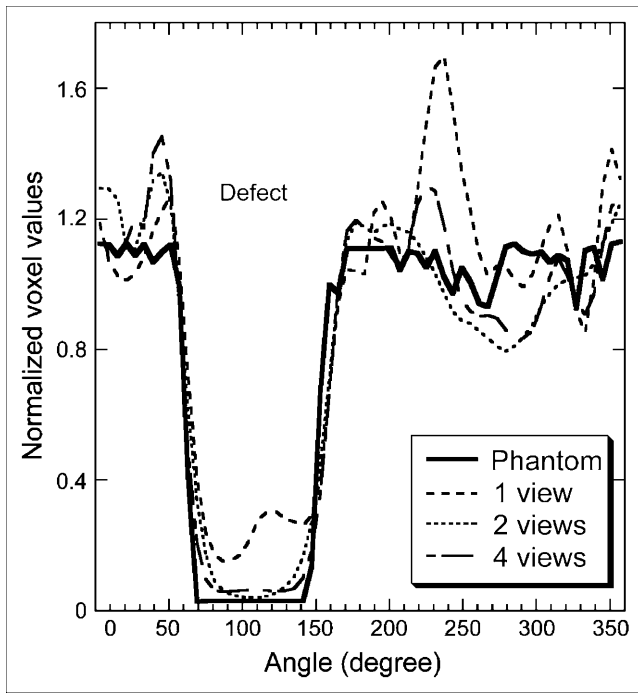


**FIGURE 5.** Circumferential profile curves for slice 36 of digital phantom and reconstructed images with 1, 2, and 4 views.

clipped views of the myocardium. Positioning procedures are potentially very time consuming and could easily reduce the predicted time advantage significantly. Successful implementation of multipinhole imaging in a clinical setting will depend critically on how well these positioning procedures can be optimized.

We have shown that increasing the angular sampling of the heart will significantly reduce the severity of the artifacts that arise from the classic single-detector multipinhole technique. Our results qualitatively agree with a simulation study of Koral et al. (39), who have shown as early as 1982 that adding an orthogonal view to a standard 7-pinhole acquisition could significantly improve the image quality and reduce the blurring along the long axis of the heart.

Although increased angular sampling improves the image quality significantly, the ultimate challenge for multipinhole imaging will be how well the diagnostic accuracy (lesion detection performance) of MPI studies performed with standard parallel-hole collimators can be matched or exceeded. In particular, multipinhole imaging is more prone to formation of artifacts because it inherently produces an incomplete tomographic dataset. Another potential drawback of this technique is the limited field of view of the multipinhole collimators. Background activity from other organs, especially if this activity is not seen by all views, could cause severe problems. Future work must address these issues very carefully to guarantee that the diagnostic quality of MPI is not compromised.

In the midst of these important questions, multipinhole imaging presents the potential to significantly improve patient care and management in a way that also may enable

us to perform novel acquisition protocols that cannot be performed currently with parallel-hole collimators. For example, dynamic imaging studies, such as tracer uptake or clearance in the myocardium, are feasible using stationary detectors with multipinhole collimators that provide sufficient angular sampling. We have shown that acquisition with 2 views produces tomograms with high image quality. Data acquisition therefore could be performed with a stationary dual-head camera, making it possible to perform time-dependent studies without moving or rotating the camera during the acquisition.

Finally, as mentioned earlier, multipinhole collimators can be designed to maximize spatial resolution and thereby offer a potentially important approach of imaging radio-labeled molecular agents. Our study indicates that spatial resolution can be improved by at least 2-fold with the current multipinhole collimator design at a detection efficiency comparable to that of a parallel-hole collimator and therefore could improve the use of novel molecular imaging agents in situations in which improved spatial resolution is crucial.

## CONCLUSION

SPECT is an important clinical method for performing MPI and its significance likely will increase with the advent of new and novel molecular imaging agents. For that reason it is desirable to improve the detection efficiency of SPECT at comparable or higher spatial resolution than SPECT with conventional parallel-hole collimators. In this study, we have shown that multipinhole MPI has significant potential for improving detection efficiency and spatial resolution and, in this way, offers significant promise for meeting the challenges and expectations in the age of molecular imaging and multimodality imaging techniques. This approach also facilitates the process of imaging dynamically changing radionuclide distributions.

The work presented here describes a means to increase the detection efficiency of myocardial SPECT. We have compared the image quality and detection efficiency of a stationary multipinhole imaging system with a rotating parallel-hole collimator and find that the detection efficiency of a multipinhole imaging system is about a 5-fold higher with the same spatial resolution as a LEHR parallel-hole collimator. Traditionally, multipinhole MPI has been performed with a single view using a 7- or 9-pinhole collimator, which incurs artifacts due to undersampling. The work presented here shows in computer simulations that performing multipinhole imaging with 2–4 views can significantly improve the quality of the reconstructed image from that obtained with just a single view.

Therefore, we conclude that multipinhole MPI offers significant advantages over rotational SPECT with conventional parallel-hole collimators. Therefore, it is worthwhile to further investigate multipinhole collimators for tomographic MPI of single-photon radiopharmaceuticals.

## ACKNOWLEDGMENTS

We are grateful for financial support by a University of California Campus–Laboratory Collaboration Program (CLC-01-54). This work is also supported by a Bioengineering Research Partnership award from the National Institute of Biomedical Imaging and Bioengineering, by National Institutes of Health (NIH) grant 8 R01 EB00348, and by a Small Business Innovative Research award from the National Heart, Lung and Blood Institute, NIH grant 9 R44 HL 078295-02.

## REFERENCES

- Underwood SR, Shaw LJ, Anagnostopoulos C, et al. Myocardial perfusion scintigraphy and cost effectiveness of diagnosis and management of coronary heart disease. *Heart*. 2004;90(suppl 5):v34–v36.
- Beller GA. First annual Mario S. Verani, MD, memorial lecture: clinical value of myocardial perfusion imaging in coronary artery disease. *J Nucl Cardiol*. 2003;10:529–542.
- Luechinger R, Zeijlemaker VA, Pedersen EM, et al. In vivo heating of pacemaker leads during magnetic resonance imaging. *Eur Heart J*. 2005;26:325–327.
- Rozner MA, Burton AW, Kumar A. Pacemaker complication during magnetic resonance imaging. *J Am Coll Cardiol*. 2005;45:161–162.
- Garber AM, Solomon NA. Cost-effectiveness of alternative test strategies for the diagnosis of coronary artery disease. *Ann Intern Med*. 1999;130:719–728.
- Pollock SG, Abbott RD, Boucher CA, Beller GA, Kaul S. Independent and incremental prognostic value of tests performed in hierarchical order to evaluate patients with suspected coronary artery disease: validation of models based on these tests. *Circulation*. 1992;85:237–248.
- Underwood SR, Godman B, Salyani S, Ogle JR, Ell PJ. Economics of myocardial perfusion imaging in Europe: the EMPIRE Study. *Eur Heart J*. 1999;20:157–166.
- Mark DB, Shaw LJ, Lauer MS, O'Malley PG, Heidenreich P. 34th Bethesda Conference: Task force #5—Is atherosclerosis imaging cost effective? *J Am Coll Cardiol*. 2003;41:1906–1917.
- Hachamovitch R, Berman DS, Kiat H, Cohen I, Friedman JD, Shaw LJ. Value of stress myocardial perfusion single photon emission computed tomography in patients with normal resting electrocardiograms: an evaluation of incremental prognostic value and cost-effectiveness. *Circulation*. 2002;105:823–829.
- Hachamovitch R, Hayes S, Friedman JD, et al. Determinants of risk and its temporal variation in patients with normal stress myocardial perfusion scans: what is the warranty period of a normal scan? *J Am Coll Cardiol*. 2003;41:1329–1340.
- Klocke FJ, Baird MG, Lorell BH, et al. ACC/AHA/ASNC guidelines for the clinical use of cardiac radionuclide imaging: executive summary—a report of the American College of Cardiology/American Heart Association Task Force on Practice Guidelines (ACC/AHA/ASNC Committee to Revise the 1995 Guidelines for the Clinical Use of Cardiac Radionuclide Imaging). *Circulation*. 2003;108:1404–1418.
- Davies JR, Rudd JH, Weissberg PL. Molecular and metabolic imaging of atherosclerosis. *J Nucl Med*. 2004;45:1898–1907.
- Meoli DF, Sadeghi MM, Krassilnikova S, et al. Noninvasive imaging of myocardial angiogenesis following experimental myocardial infarction. *J Clin Invest*. 2004;113:1684–1691.
- Blankenberg FG, Strauss HW. Nuclear medicine applications in molecular imaging. *J Magn Reson Imaging*. 2002;16:352–361.
- Winnard P Jr, Raman V. Real time non-invasive imaging of receptor-ligand interactions in vivo. *J Cell Biochem*. 2003;90:454–463.
- Schramm NU, Ebel G, Engeland U, Schurrat T, Behe M, Behr TM. High-resolution SPECT using multipinhole collimation. *IEEE Trans Nucl Sci*. 2003;50:315–320.
- Beekman FJ, Vastenhout B. Design and simulation of a high-resolution stationary SPECT system for small animals. *Phys Med Biol*. 2004;49:4579–4592.
- Koral KF, Rogers WL. Application of ART to time-coded emission tomography. *Phys Med Biol*. 1979;24:879–894.
- Koral KF, Rogers WL, Knoll GF. Digital tomographic imaging with time-modulated pseudorandom coded aperture and Anger camera. *J Nucl Med*. 1975;16:402–413.
- Rogers WL, Koral KF, Mayans R, et al. Coded-aperture imaging of the heart. *J Nucl Med*. 1980;21:371–378.
- Barrett H. Fresnel zone plate imaging in nuclear medicine. *J Nucl Med*. 1972;13:382–385.
- Simpson RG, Barrett HH, Fisher HD. Decoding techniques for use with annular coded apertures. In: Marom E, Friesem AA, Wiener-Avnear E, eds. *Applications of Holography and Optical Data Processing*. Pergamon: Oxford, U.K.; 1977:119–128.
- Kujoory MA, Miller EL, Barrett HH, Gindi GR, Tamura PN. Coded aperture imaging of gamma-ray sources with an off-axis rotating slit. *Appl Opt*. 1980;19:4186–4195.
- Vogel RA, Kirch D, LeFree M, Steele P. A new method of multiplanar emission tomography using a seven pinhole collimator and an Anger scintillation camera. *J Nucl Med*. 1978;19:648–654.
- Rollo FD, Patton JA. Perspectives on seven pinhole tomography. *J Nucl Med*. 1980;21:888–890.
- Chang W, Henkin RE. Seven-pinhole multigated tomography and its application to blood-pool imaging: technical parameters. *J Nucl Med*. 1980;21:682–688.
- Mullani NA, Gould KL, Gaeta JM. Tomographic imaging of the heart with thallium-201: seven-pinhole or rotating gamma camera? *J Nucl Med*. 1981;22:925–926.
- Tamaki N, Yonekura Y, Mukai T, et al. Clinical evaluation of emission tomography using seven-pinhole collimator: improved detection of perfusion defect by the addition of the right anterior oblique projection. *Clin Nucl Med*. 1982;7:157–160.
- Vogel RA. Seven-pinhole tomography: curiosity or clinically useful technique? *Clin Nucl Med*. 1982;7:193–194.
- Bateman T, Garcia E, Maddahi J, et al. Clinical evaluation of seven-pinhole tomography for the detection and localization of coronary artery disease: comparison with planar imaging using quantitative analysis of myocardial thallium-201 distribution and washout after exercise. *Am Heart J*. 1983;106:263–271.
- Myers MJ, Sokole EB, de Bakker J. A comparison of rotating slant hole collimator and rotating camera for single photon emission tomography of the heart. *Phys Med Biol*. 1983;28:581–588.
- Wagner S, Kopka K, Law MP, et al. Synthesis and first in vivo evaluation of new selective high affinity beta1-adrenoceptor radioligands for SPECT based on ICI 89,406. *Bioorg Med Chem*. 2004;12:4117–4132.
- Kopka K, Wagner S, Riemann B, et al. Design of new beta1-selective adrenoceptor ligands as potential radioligands for in vivo imaging. *Bioorg Med Chem*. 2003;11:3513–3527.
- Miyagawa M, Beyer M, Wagner B, et al. Cardiac reporter gene imaging using the human sodium/iodide symporter gene. *Cardiovasc Res*. 2005;65:195–202.
- Philips Medical Systems. Product information. [http://www.medical.philips.com/main/products/nuclearmedicine/assets/images/cardiomd/CardioMD\\_DS\\_01\\_15\\_04.pdf](http://www.medical.philips.com/main/products/nuclearmedicine/assets/images/cardiomd/CardioMD_DS_01_15_04.pdf). Accessed January 31, 2006.
- Sunyaung J, Jaszczak RJ, Tsui BMW, et al. ROC evaluation of SPECT myocardial lesion detectability with and without nonuniform attenuation compensation using an anthropomorphic female phantom. *Nucl Sci Symp Med Imaging Conf Rec*. 1997;2:998–1002.
- Segars WP, Lalush DS, Tsui BMW. A realistic spline-based dynamic heart phantom. *IEEE Trans Nucl Sci*. 1999;46:503–506.
- Segars WP. *Development of a New Dynamic NURBS-Based Cardiac-Torso (NCAT) Phantom* [PhD thesis]. Chapel Hill, NC: University of North Carolina; 2001.
- Koral KF, Clinthorne NH, Rogers WL, Keyes JW Jr. Feasibility of sharpening limited-angle tomography by including an orthogonal set of projections. *Nuclear Instrum Methods*. 1982;193:223–227.